Acta Biomaterialia 7 (2011) 809–820

Contents lists available at ScienceDirect

Acta Biomaterialia

journal homepage: www.elsevier.com/locate/actabiomat

Biomimetic composite coating on rapid prototyped scaffolds for bone tissue engineering

M. Tarik Arafat [a,c], Christopher X.F. Lam [b], Andrew K. Ekaputra [b], Siew Yee Wong [c], Xu Li [c,*], Ian Gibson [a,d,*]

[a] Department of Mechanical Engineering, National University of Singapore, Singapore 117576, Singapore
[b] Division of Bioengineering, National University of Singapore, Singapore 119260, Singapore
[c] Institute of Materials Research and Engineering, A*STAR (Agency for Science, Technology and Research), 3 Research Link, Singapore 117602, Singapore
[d] Laboratory for Rapid and Sustainable Product Development, Institute Politechnic Leiria, Leiria, Portugal

ARTICLE INFO

Article history:
Received 4 July 2010
Received in revised form 4 September 2010
Accepted 8 September 2010
Available online 16 September 2010

Keywords:
Rapid prototyping scaffolds
Biomimetic composite coating
Carbonated hydroxyapatite–gelatin composite
Bone tissue engineering

ABSTRACT

The objective of this present study was to improve the functional performance of rapid prototyped scaffolds for bone tissue engineering through biomimetic composite coating. Rapid prototyped poly(ε-caprolactone)/tri-calcium phosphate (PCL/TCP) scaffolds were fabricated using the screw extrusion system (SES). The fabricated PCL/TCP scaffolds were coated with a carbonated hydroxyapatite (CHA)–gelatin composite via biomimetic co-precipitation. The structure of the prepared CHA–gelatin composite coating was studied by scanning electron microscopy (SEM), X-ray photoelectron spectroscopy and Fourier transform infrared spectroscopy. Compressive mechanical testing revealed that the coating process did not have any detrimental effect on the mechanical properties of the scaffolds. The cell–scaffold interaction was studied by culturing porcine bone marrow stromal cells (BMSCs) on the scaffolds and assessing the proliferation and bone-related gene and protein expression capabilities of the cells. Confocal laser microscopy and SEM images of the cell–scaffold constructs showed a uniformly distributed cell sheet and accumulation of extracellular matrix in the interior of CHA–gelatin composite-coated PCL/TCP scaffolds. The proliferation rate of BMSCs on CHA–gelatin composite-coated PCL/TCP scaffolds was about 2.3 and 1.7 times higher than that on PCL/TCP scaffolds and CHA-coated PCL/TCP scaffolds, respectively, by day 10. Furthermore, reverse transcription polymerase chain reaction and Western blot analysis revealed that CHA–gelatin composite-coated PCL/TCP scaffolds stimulate osteogenic differentiation of BMSCs the most, compared with PCL/TCP scaffolds and CHA-coated PCL/TCP scaffolds. These results demonstrate that CHA–gelatin composite-coated rapid prototyped PCL/TCP scaffolds are promising for bone tissue engineering.

1. Introduction

Scaffold-based bone tissue engineering aims to aid in the repair and/or regeneration of bone defects by using a scaffold as a platform for carrying cells or therapeutic agents to the site of interest. An ideal scaffold aims to mimic the mechanical and biochemical properties of the native tissue. In order to effectively achieve these properties a scaffold should have a suitable architecture favouring the flow of nutrients for cell growth. It should also have osteoconductive properties, supporting cells through a suitable surface chemistry [1–3].

Rapid prototyping (RP) technologies are fast becoming the technologies of choice for fabricating scaffolds for bone tissue engineering due to the reliability, high degree of reproducibility and potential to overcome the limitations of conventional manual-based fabrication techniques [4]. Complex scaffold architecture designs based on a hierarchical approach can be readily fabricated through RP [5,6]. The screw extrusion system (SES) is a promising RP technique which has been used to fabricate both polymer and polymer/ceramic composite scaffolds [7,8]. Polymer/ceramic composite scaffolds are preferable candidates for bone tissue engineering because they integrate the favourable properties of both the polymer and ceramic and, hence, show enhanced mechanical properties and biocompatibility [8–10]. However, blending the ceramic with the polymer directly may lead to masking of the ceramic particles by polymer. This limits exposure of the ceramic on the scaffold surface and hinders direct contact between cells and the bioactive ceramic particles and thus diminishes the osteoconductive properties offered by them. Therefore, in order to improve the osteoconductive properties of polymer/ceramic composite scaffolds, coating a layer of ceramic on the scaffold surface is

* Corresponding authors at: Institute of Materials Research and Engineering, A*STAR, 3 Research Link, Singapore 117602, Singapore. Tel.: +65 68748421; fax: +65 68727528 (X. Li); Department of Mechanical Engineering, NUS, Singapore 117576, Singapore. Tel.: +65 92777343; fax: +65 67791495 (I. Gibson).
E-mail addresses: x-li@imre.a-star.edu.sg (X. Li), mpegi@nus.edu.sg (I. Gibson).

1742-7061/$ - see front matter © 2010 Acta Materialia Inc. Published by Elsevier Ltd. All rights reserved.
doi:10.1016/j.actbio.2010.09.010

considered an efficient approach. It should be noted that an ideal surface coating can provide desirable biological properties to the bulk implant, while retaining the structural properties of the scaffold.

Among various coating approaches, the biomimetic approach acts in a more efficient and similar way to the natural system [11]. Kokubo et al. first reported the use of simulated body fluid (SBF) for biomimetic growth of apatite coatings on bioactive $CaO–SiO_2$ glasses by mimicking the natural biomineralization process [12]. However, this conventional biomimetic process shows some limitations, notably the time consuming nature of the process, which may take several weeks [13,14]. Though the process time could be shortened by using concentrated SBF, it still requires a constant pH and replenishment of the concentrated SBF frequently to maintain supersaturation for apatite crystal growth [15]. Therefore, an alternative, simple and efficient approach for biomimetic coating is required.

A previous study on RP scaffolds coated with apatite did not produce promising results, due to flaking of the thick apatite layer on the bars of the scaffolds [16]. To reduce the tendency to flake a composite coating may be desirable, as a recent study showed that collagen can improve both the cohesive and adhesive properties of an apatite coating on titanium with a significantly higher coating retention for the apatite–collagen composite coating compared with an apatite coating [17]. However, relatively little work has been reported on apatite–collagen composite coatings on polymer-related scaffolds [18]. More specifically, there is no study of such composite coatings on RP scaffolds.

In comparison with collagen, the collagen derivative gelatin has a high number of biological functional groups and, as gelatin is denatured, overcomes the possible concerns about immunogenicity associated with collagen. Moreover, its cost efficiency can facilitate its selection over collagen. Previous studies have reported the use of hydroxyapatite (HA)–gelatin composites as a scaffold for bone tissue engineering [19–21]. It was found that osteoblast stimulation was significantly higher on co-precipitated HA–gelatin scaffolds than on pure gelatin or conventional HA–gelatin scaffolds prepared by directly mixing the gelatin with HA [20]. However, biological apatites always contain carbonate functional groups. Carbonated hydroxyapatite (CHA) implants exhibit greater osteoconductive properties and earlier bioresorption compared with HA samples [22]. Therefore, we hypothesize that the combination of CHA and gelatin as a composite coating through biomimetic co-precipitation has the potential to be an effective biomimetic coating for bone tissue engineering.

The objective of the present study was to develop a facile but efficient approach to provide a biomimetic composite coating on rapid prototyped scaffolds for bone tissue engineering. Rapid prototyped poly(ε-caprolactone)/tri-calcium phosphate (PCL/TCP) scaffolds were fabricated using an in-house SES. The CHA–gelatin composite coating was then formed on the fabricated PCL/TCP scaffolds through biomimetic co-precipitation. CHA-coated scaffolds were also prepared in order to understand the influence of gelatin incorporation on cell proliferation and differentiation activity. The scaffolds were evaluated for surface morphology, composition and compressive modulus. The biological capabilities of these scaffolds were also evaluated by culturing porcine bone marrow stromal cells (BMSCs) on them.

2. Materials and methods

2.1. Materials

Poly(ε-caprolactone) (PCL) (M_n 80,000), gelatin (type A, from porcine skin), calcium chloride ($CaCl_2$), phosphoric acid (H_3PO_4, 85% solution in water), sodium carbonate (Na_2CO_3), acetic acid (CH_3COOH), sodium hydroxide (NaOH) and potassium hydrophosphate (K_2HPO_4) were purchased from Sigma–Aldrich (Singapore). Tri-calcium phosphate (TCP) was obtained from Progentix (The Netherlands).

2.2. Fabrication of PCL/TCP scaffolds by SES

A PCL/TCP composite with 20 wt.% TCP was prepared by blending TCP powder into PCL using a Brabender Mixer at 80 °C. Rapid prototyped PCL/TCP scaffolds were then fabricated from the prepared PCL/TCP composite using an in-house SES with a nozzle diameter of 0.4 mm at a processing temperature of 85 °C [8,23]. Each layer of the scaffolds was fabricated with a designed scaffold pattern of 0°/60°/120° orientation. The size of the scaffolds used for the mechanical test was $5 \times 5 \times 8$ mm and that for cell culture $5 \times 5 \times 3.5$ mm.

2.3. Surface coating on PCL/TCP scaffolds

The fabricated PCL/TCP scaffolds were first treated in 10 ml of 5 M NaOH at room temperature for 12 h, followed by thorough washing with deionized water to remove the free NaOH. The NaOH-treated scaffolds were then dipped alternately into calcium chloride solution and potassium hydrophosphate solution to obtain a $CaHPO_4$ coating as a nucleation site for the next CHA coating or CHA–gelatin composite coating [24]. In brief, the NaOH-treated scaffolds were dipped in 20 ml of 0.2 M $CaCl_2$ aqueous solution for 10 min and then dipped in deionized water for 5 s, followed by air drying for 3 min. The sample was subsequently dipped in 20 ml of 0.2 M K_2HPO_4 aqueous solution for 10 min and then dipped in deionized water for 5 s, followed by air drying for 3 min. The whole process was repeated three times.

The $CaHPO_4$-coated scaffolds were immersed in 20 ml of 0.1 M CH_3COOH and then 10 ml of 0.1 M $CaCl_2$ and 6 ml of 0.1 M H_3PO_4 (Ca/P = 1.66) were dropped slowly through separate syringe pumps under stirring. The pumps were adjusted to keep the ratio of Ca/P at 1.66. After further stirring for 30 min, 18 ml of 0.1 M Na_2CO_3 with the molar ratio of $CO_3^{2-}/PO_4^{3-} = 3$ was gradually added. The mixture was stirred for another 30 min and then the pH of the mixture was adjusted to 9 using 0.1 M NaOH. The CHA-coated PCL/TCP scaffolds (PCL/TCP–CHA) were collected after ageing the solution for 3 h. Finally, the scaffolds were thoroughly washed with deionized water and freeze dried.

To prepare CHA–gelatin composite-coated PCL/TCP scaffolds (PCL/TCP–CHA–gelatin) first 40 mg gelatin was dissolved into 20 ml of deionized water at 37 °C to obtain a stock gelatin solution (2 mg ml^{-1}). Then $CaHPO_4$-coated scaffolds were dipped in the above gelatin solution for 0.5 h, followed by washing with deionized water to remove free gelatin. The gelatin-coated scaffolds were then immersed in 20 ml of 0.1 M CH_3COOH solution containing 40 mg gelatin. Finally, the CHA–gelatin composite was coated onto the gelatin-treated PCL/TCP scaffolds by adding $CaCl_2$ and H_3PO_4, following the same process as for CHA coating.

2.4. Scaffold characterization

The surface morphology of the scaffolds was observed by field emission scanning electron microscopy (SEM) (Philips XL30 FEG) at a beam intensity of 10 keV. Scaffolds were gold sputtered using a JEOL fine sputter coater (JFC-1200) for 20 s at 10 mA before observation. The thickness of the CHA and CHA–gelatin composite coatings were measured from cross-sectional SEM images of filaments in the coated scaffolds. Attenuated total refraction Fourier transform infrared spectroscopy (ATR-FT-IR) analysis of the coatings was performed in an Avatar 380 (Thermo Nicolet) over a range

of 800–1800 cm^{-1} at resolution of 2 cm^{-1} to study the chemical structure of the coatings. The water contact angles of the coatings were measured by the sessile method at 25 °C in an air atmosphere using an NRL-100-00-(230) contact angle goniometer (Rame-Hart Inc.). ATR-FT-IR testing and water contact angle measurements were carried out with film samples assuming that the coatings on both films and scaffolds were similar. The films for testing were prepared by hot pressing the PCL/TCP composite and then following the same coating process as for the scaffolds. X-ray photoelectron spectroscopy (XPS) (Thetaprobe, Thermo Scientific) was used to study the scaffold surface. A monochromated AlK_α (1486.6 eV) electron source was used along with a flood gun for surface charge compensation (energy 2 eV, emission current 100 mA). The detector was set to standard lens mode constant analyzer energy (CAE), with a passed energy for the survey spectra of 200 eV and for the high resolution spectra of 40 eV. Data analysis was carried out using Avantage software.

2.5. Compression testing

Compression testing of the scaffolds was conducted using an Instron 4502 uniaxial testing system with a 1 kN load cell. Scaffolds with a size of 5 × 5 × 8 mm and 0°/60°/120° orientation pattern were compressed at a rate of 1 mm min^{-1} up to a strain level of approximately 80%. The stress–strain (σ–ε) curves were obtained and the compressive modulus was calculated from the stress–strain curve as the slope of the initial linear portion of the curve, with any toe region due to the initial settling of the specimen neglected. Five scaffolds for each group were tested and measurements are reported as means ± standard deviation. Compression testing was also carried out under simulated physiological conditions by keeping the scaffolds at 37 °C in phosphate-buffered saline (PBS) for 24 h before testing.

2.6. Cell seeding on scaffolds

Dulbecco's modified Eagle's medium (DMEM), fetal bovine serum (FBS) and penicillin–streptomycin (pen-strep) were purchased from Gibco. Trypsin–EDTA was purchased from Thermo Scientific Hyclone.

Cryopreserved porcine BMSCs (passage 2), previously isolated from the iliac crest of pigs, were plated and expanded in T75 tissue culture flasks in DMEM supplemented with 10% FBS and 1% antibiotics until sufficient cells were obtained (not beyond passage 4). The medium was changed twice per week and cells were detached using trypsin–EDTA and passaged into fresh culture flasks at a ratio of 1:3 upon reaching confluence. Cultures were incubated at 37 °C in a humidified atmosphere containing 95% air and 5% CO_2.

First, the scaffolds were sterilized with 70% ethanol for 30 min and then further sterilized under UV light for 30 min, followed by drying under sterile conditions at room temperature for 2 h. Three groups of scaffolds were prepared, PCL/TCP, PCL/TCP–CHA and PCL/TCP–CHA–gelatin. Each scaffold was seeded with approximately 1.8×10^5 BMSCs. The cell–scaffold constructs were cultured in 24-well tissue culture plates for up to 10 days in growth medium and at specific time points assessed and observed for proliferation. After 10 days culture in growth medium an osteogenic cocktail of 10 nM dexamethasome, 50 μM ascorbic acid and 10 mM of β-glycerolphosphate (Sigma) was added to induce osteogenesis. The cell–scaffold constructs were further cultured for 21 days after induction and samples retrieved and assessed at specific time points for gene and protein expression.

2.7. Morphology of the cell–scaffold constructs

Confocal laser microscopy and SEM were used to assess cell viability, morphology and attachment in vitro. Cells were stained with 2 μg ml^{-1} fluorescein diacetate (FDA) (1 mg ml^{-1}, Molecular Probes) to stain the cytoplasm of live cells fluorescent green. During FDA staining samples were incubated at 37 °C for 15 min, followed by rinsing with PBS. Cells were then counterstained with 5 μg ml^{-1} propidium iodide (PI) (1 mg ml^{-1}, Molecular Probes) to stain the nucleus of dead cells fluorescent red. During PI staining the samples were kept at room temperature for 2 min and then rinsed with PBS. These samples were mounted for viewing under a confocal laser microscope (IX 70, Olympus). Depth projection images were constructed from up to 30 horizontal image sections (12 μm each) through the stained cell–scaffold constructs using FV1000 Viewer (Ver.1.7a) software. After confocal imaging cell–scaffold constructs were fixed in 10% formalin overnight and then dehydrated through a series of graded ethanol solutions (5%, 10%, 20%, 40%, 60%, 80%, 90% and 100%), each for 10 min. Finally, the samples were dried overnight at room temperature. Dried cellular constructs were gold sputtered and observed by SEM at an accelerating voltage of 10 keV.

2.8. PicoGreen® assay

Proliferation of BMSCs in cell–scaffold constructs were studied using the PicoGreen® assay as per the manufacturer's protocol (Molecular Probes PicoGreen dsDNA Quantitation Kit). Total DNA from cells in the constructs were extracted via freeze–thaw cycles. DNA levels in the cell lysates were then assayed using the DNA binding dye PicoGreen® followed by spectrophotometry quantification.

2.9. Reverse transcription polymerase chain reaction (RT-PCR)

At specified time points the cell–scaffold constructs were lysed with Trizol (Invitrogen) and thoroughly vortexed. The samples in Trizol were stored at −80 °C until RNA isolation. Total RNA was isolated using the RNeasy Mini Kit (Qiagen) with RNase-Free DNase (Qiagen) according to the manufacturer's protocol.

Reverse transcription was performed with a QuantiTect Reverse Transcriptase Kit (Qiagen) to produce the required cDNA. Quantitative PCR was performed for the quantification of gene expression using the primers listed in Table 1 and a QuantiTect SYBR Green PCR Kit (Qiagen) in a Mx3000P Real-Time PCR System (Stratagene). Target genes were normalized against GAPDH expression.

2.10. Western blotting

Protein extracts were harvested from the cell–scaffold constructs with ice-cold radio-immunoprecipitation assay (RIPA) buffer (Thermo Scientific). Protein lysates were purified and concentrated using NanoSep columns (Pall 3 K). Total protein quantity was quantified using the microBCA assay (Pierce) as per the manufacturer's protocol. Proteins were denatured at 90 °C for 5 min, resolved by 10% sodium dodecyl sulphate polyacrylamide gel electrophoresis and transferred to nitrocellulose membranes (Bio-Rad). After blocking with 1% non-fat milk in tris-buffered saline (TBS) for 1 h the membranes were incubated for 1 h with primary antibodies for polyclonal rabbit-anti-human β-actin (Delta Biolabs), osteonectin (ON), osteocalcin (OCN) (Santa Cruz) or osteopontin (OPN) (Abcam). The primary antibodies were diluted from 1:500 to 1:2000 in TBS

Table 1
Forward primers and reverse primers used in RT-PCR.

Gene ID	Forward primer	Reverse primer
GAPDH	GCTTTGCCCCGCGATCTAATGTTC	GCCAAATCCGTTCACTCCGACCTT
CBFA1	GAGGAACCGTTTCAGCTTACTG	CGTTAACCAATGGCACGAG
COL1	CCAAGAGGAGGGCCAAGAAGAAGG	GGGGCAGACGGGGCAGCACTC
OCN	TCAACCCCGACT GCGACGAG	TTGGAGCAGCTG GGATGATGG

with 0.1% Tween (TBST). After three washes with TBST the membranes were next incubated with rabbit anti-goat horseradish peroxidase-conjugated secondary IgG (Zymed) at 1:15,000 for 1 h, followed by another three washes with TBST. Immunoreactive bands were visualised and detected using the SuperSignal Chemiluminescent reagent (Pierce) and a VersaDoc Imaging System (Bio-Rad). The intensities of the bands were quantitatively analyzed using densitometry (Quantity-One, Bio-Rad). Target proteins were normalized against β-actin expression.

2.11. Statistical analysis

An unpaired Student's *t*-test was performed to evaluate the significance of the observed differences between the study groups. A value of $P < 0.05$ was considered to be statistically significant. Data were tested for normality prior to performing the Student's *t*-test.

3. Results and discussion

3.1. Scaffold fabrication

SES, a computer controlled fabrication process, is fast becoming the technology of choice in automating scaffold production to produce specifically tailored pore geometries and architectural patterns [8]. In the present study bioresorbable PCL/TCP scaffolds were fabricated using SES with the following structural properties: (i) 100% pore interconnectivity with a pore size of ~500 μm; (ii) a scaffold porosity of 65%; (iii) a 0°/60°/120° lay down pattern. The architectural layout of the developed scaffolds resembles a honeycomb, which is advantageous over a foam type structure. It has been reported that honeycomb structures allow bone in-growth in the later stages [25,26], whereas a foam structure limits tissue growth, confining it to the surface of the foam [27,28].

3.2. Biomimetic CHA–gelatin composite coating

In order to improve the osteoconductive properties of rapid prototyped PCL/TCP scaffolds a CHA–gelatin composite was coated onto them through a facile biomimetic process. Scaffolds coated with CHA alone were also prepared to verify the improvement in performance of scaffolds due to the incorporated gelatin. To promote biomimetic mineralization on the surface of PCL/TCP scaffolds with a CHA or CHA–gelatin composite coating $CaHPO_4$ was coated onto the scaffold first, to induce surface nucleation, as reported previously [24]. In the preparation of CHA-coated PCL/TCP scaffolds (PCL/TCP–CHA) the $CaHPO_4$-coated PCL/TCP scaffolds were immersed in CH_3COOH, followed by simultaneous dropwise addition of $CaCl_2$ and H_3PO_4 and further dropwise addition of

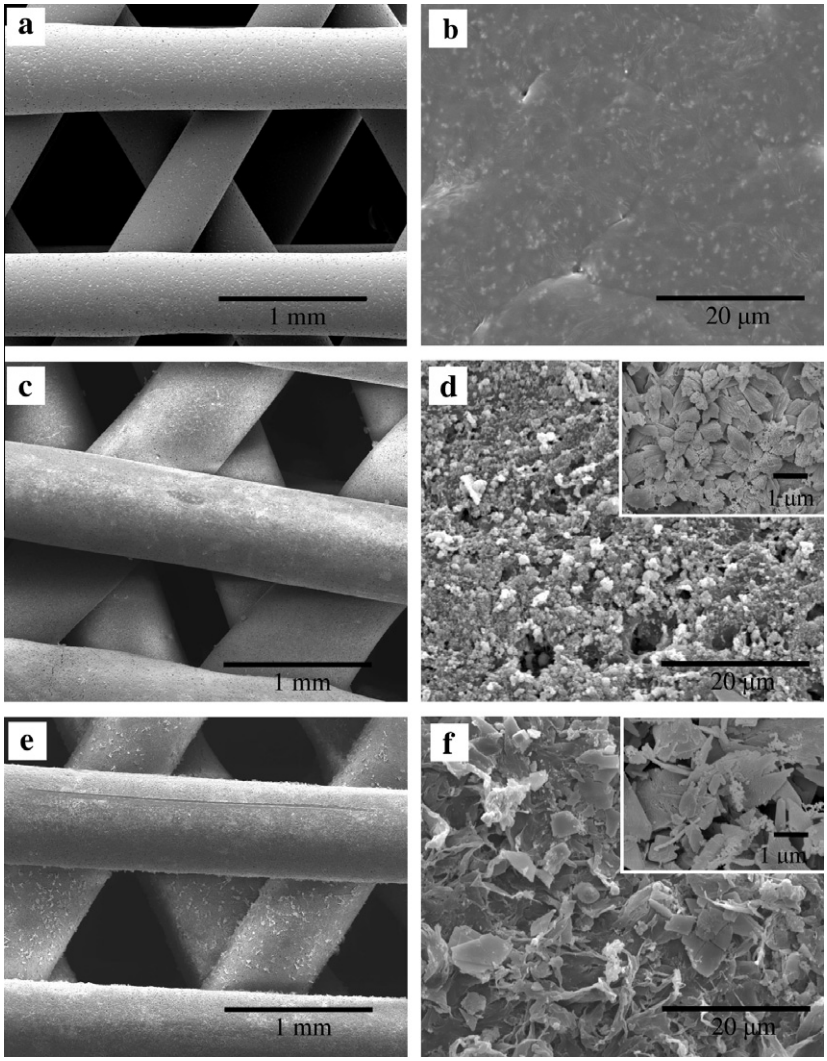

Fig. 1. SEM images of (a and b) PCL/TCP, (c and d) PCL/TCP–CHA and (e and f) PCL/TCP–CHA–gelatin scaffolds. The scale bars in the left column, right column and inset represent 1 mm, 20 and 1 μm, respectively.

Na_2CO_3 according to a previously reported procedure for CHA preparation [29]. Due to the $CaHPO_4$ nucleation CHA was coated onto the PCL/TCP scaffolds. For the CHA–gelatin composite-coated PCL/TCP scaffolds (PCL/TCP–CHA–gelatin) the $CaHPO_4$-coated PCL/TCP scaffolds were further coated with gelatin via electrostatic attraction between $CaHPO_4$ and gelatin by dipping in gelatin solution [30]. Finally, gelatin was co-precipitated with CHA on the scaffold surface to produce a CHA–gelatin composite coating via a biomimetic process similar to that for CHA coating. The carboxyl and amine groups present in gelatin may become charged groups, such as $-COO^-$ and $-NH_3^+$, under the coating conditions which can promote CHA–gelatin composite nucleation. It should be noted that the whole approach is free of gelatin cross-linking. Thus, the potential toxicity caused by chemicals employed for cross-linking gelatin in other systems can be avoided [31,32]. More interestingly, using the biomimetic approach described here can achieve a biomineralized coating in a few hours.

3.3. Scaffold characterization

PCL/TCP, PCL/TCP–CHA and PCL/TCP–CHA–gelatin scaffolds were characterized by SEM, ATR-FT-IR, XPS and water contact angle measurement. Compression testing was also conducted to determine whether there was any detrimental effect of the coating process on the compressive modulus of the scaffolds.

As shown in Fig. 1, while PCL/TCP scaffolds without a coating exhibited a smooth surface morphology, both the CHA-coated and CHA–gelatin composite-coated scaffolds appeared uniform with a rough surface morphology. The CHA-coated scaffolds were fully covered with almost globular apatite particles, whereas the CHA–gelatin-coated scaffolds were covered with plate-like apatite of slightly larger size than the CHA particles on PCL/TCP–CHA (Fig. 1d and f). The morphology difference between the CHA coating and CHA–gelatin composite coating could be due to the incorporation of gelatin in the biomimetic co-precipitation process. In the presence of gelatin mineral crystal formation could be altered. It has been reported that the adsorption of protein on the mineral surface can alter crystal nucleation and growth during the biomineralization process [33]. Fig. 2 shows SEM images of cross-sections of coated PCL/TCP filaments. From the SEM images the thickness of the CHA and CHA–gelatin composite coatings were measured as 606 ± 106 and 821 ± 53 nm, respectively.

The chemical structure of the CHA–gelatin composite coating was studied by ATR-FT-IR. Fig. 3c shows the FT-IR spectrum of pure gelatin with the characteristic amide I and II bands at 1650 and 1550 cm^{-1}, respectively. The observation of these characteristic amide bands of gelatin in the ATR-FT-IR spectrum of the CHA–gelatin composite-coated PCL/TCP films reveals the presence of gelatin in the composite coating (Fig. 3b). In the ATR-FT-IR spectra of both CHA-coated and CHA–gelatin composite-coated PCL/TCP films the characteristic bands for phosphate and carbonate groups were observed at 1039 and 1400 cm^{-1}, respectively, which are similar to those found in natural bone [34,35]. This demonstrates the formation of CHA with a bone-like chemical composition in the coating.

The chemical structure of the coating on the scaffolds surface was also studied by XPS, as shown in Fig. 4. Neither the characteristic peak of calcium nor that of phosphorous was observed in the XPS spectrum of the PCL/TCP scaffolds (Fig. 4a), suggesting that there were no TCP particles on the scaffold surface detectable using XPS. A possible reason for the limited exposure of TCP particles on the scaffold surface is that the TCP particles were masked by the polymer during mixing and/or the fabrication process, as reported previously [35]. This will hinder cells from making direct contact with the ceramic particles and, hence, reduces the bioactivity of the PCL/TCP scaffolds. Observation of the characteristic peaks of calcium and phosphorus in the XPS spectra of both the PCL/TCP–CHA and PCL/TCP–CHA–gelatin scaffolds suggests the formation of CHA on the surface of the coated PCL/TCP scaffolds. Moreover, the presence of the nitrogen peak in the spectrum of the PCL/TCP–CHA–gelatin scaffolds (Fig. 4c) confirmed the presence of gelatin in the CHA–gelatin composite coating. The quantitative elemental analysis by XPS showed that the Ca/P atomic ratios for the PCL/TCP–CHA and PCL/TCP–CHA–gelatin scaffolds were 1.55 and 1.52, respectively, which are similar to that for CHA found previously [29,36].

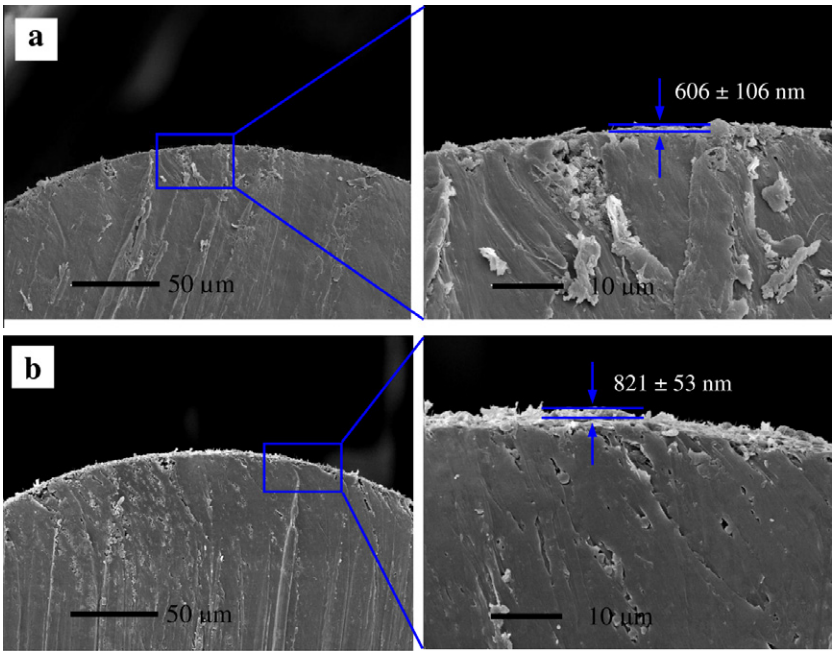

Fig. 2. SEM images of cross-sections of filaments in (a) PCL/TCP–CHA, and (b) PCL/TCP–CHA–gelatin scaffolds. The scale bars in the left column and right column represent 50 and 10 μm, respectively.

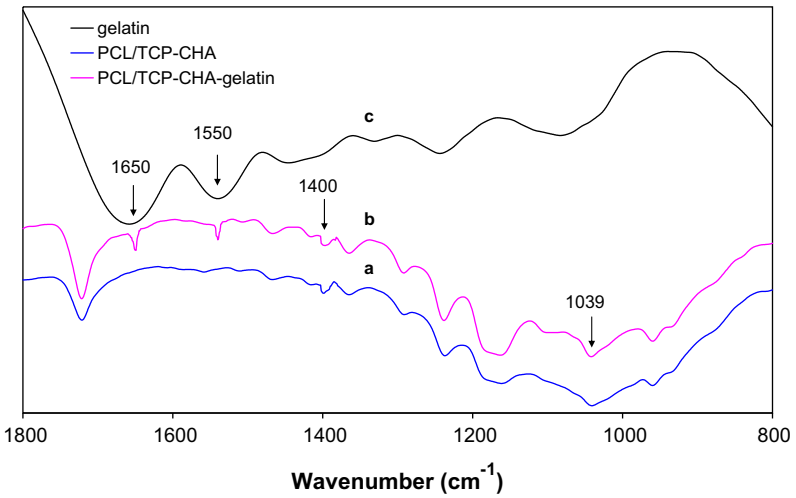

Fig. 3. ATR-FT-IR spectra of (a) CHA, and (b) CHA–gelatin composite coated PCL/TCP film and FT-IR spectra of (c) gelatin.

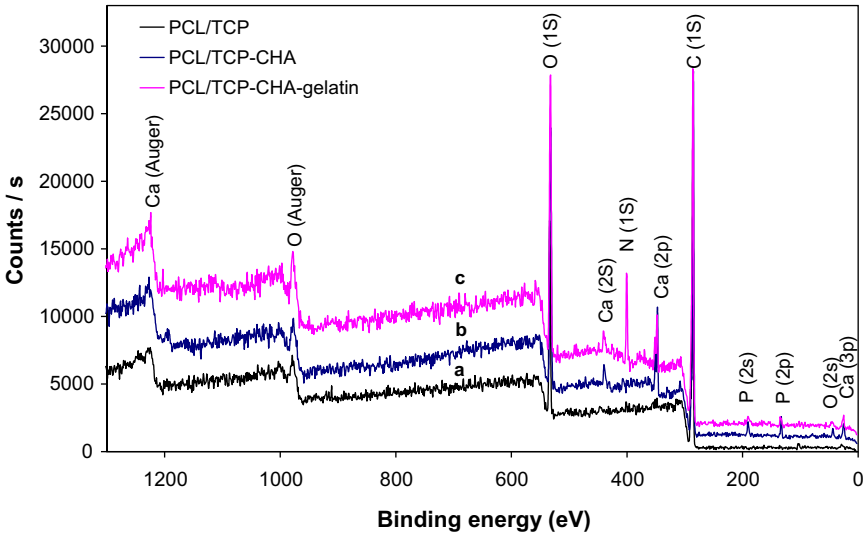

Fig. 4. XPS spectra of (a) PCL/TCP, (b) PCL/TCP–CHA, and (c) PCL/TCP–CHA–gelatin scaffolds.

The hydrophilicity of the scaffolds was tested by measuring the water contact angle of PCL/TCP films with or without coating. The water contact angle of the PCL/TCP film was 78.9°, whereas the water contact angles of the CHA-coated PCL/TCP film and CHA–gelatin composite-coated PCL/TCP film were 44.8° and 51.2°, respectively. A statistically significant ($P < 0.05$) decrease in water contact angle was found after coating, but there was no significant difference between the CHA and CHA–gelatin coatings. The contact angle test results suggest that both the CHA and CHA–gelatin composite coatings can improve the hydrophilicity of PCL/TCP scaffolds. Hydrophilic surfaces are more desirable for bone tissue engineering applications as it has been demonstrated that osteogenic cells have a higher proliferative rate on hydrophilic than on hydrophobic surfaces [37].

One of the basic functions of scaffolds for bone tissue engineering is to act as a supporting structure and provide adequate mechanical strength to maintain the spaces required for cell growth under physiological conditions. In general, SES can provide well-interconnected and highly structured scaffolds for bone tissue engineering. Here, compression testing of the scaffolds was carried out to evaluate whether there was any detrimental effect of the biomimetic coating on the mechanical properties of the scaffolds. Compression testing in the dry state revealed that the CHA and CHA–gelatin coatings increased the compressive modulus of the scaffolds by around 29% (Fig. 5). Moreover, compression testing of the scaffolds under simulated physiological conditions revealed that the modulus of the PCL/TCP scaffolds decreased by 15% compared with that in the dry state, whereas the coated scaffolds decreased by less than 10%. The compressive modulus of the coated scaffolds in the simulated physiological state was still higher than that of PCL/TCP scaffolds in the dry state. There was no significant difference in the compressive modulus between the PCL/TCP–CHA and PCL/TCP–CHA–gelatin scaffolds. This indicates that CHA and CHA–gelatin coating does not have any detrimental effect on the compressive modulus of the scaffolds in either the dry or simulated physiological states.

3.4. In vitro cell responses

Since tissue engineering scaffolds are designed to support the growth of tissues, the primary cell–scaffold interaction is extremely important. The surface of the scaffolds must be conducive to not only facilitate cell proliferation in the initial phase, but also promote cell differentiation. BMSCs are a valuable therapeutic tool

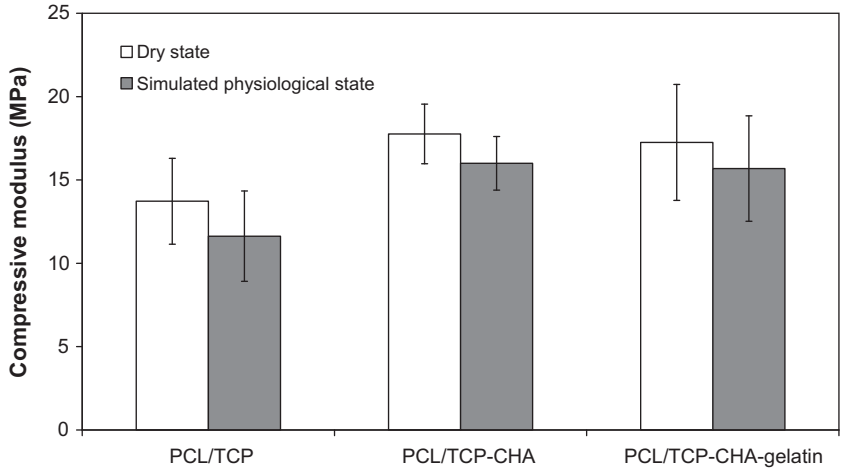

Fig. 5. Compression modulus of PCL/TCP, PCL/TCP–CHA and PCL/TCP–CHA–gelatin scaffolds in the dry and simulated physiological states.

in bone tissue engineering, since they have the capability for self-renewal and the potential for multilineage differentiation [38]. Moreover, even though they hold a similar potential to embryonic stem cells they are less associated with ethical issues and the risk of tumorigenesis [38]. Therefore, in this study the influence of scaffold surface properties was evaluated on the morphology, proliferation and gene and protein expression of BMSCs cultured on the scaffolds.

As shown in the SEM images, on day 7 BMSCs had an elongated morphology on the PCL/TCP–CHA and PCL/TCP–CHA–gelatin scaffolds, whereas the cells had a rounded morphology on the PCL/TCP scaffolds (Fig. 6). This indicates that BMSCs adhered to and grew and proliferated better on the coated scaffolds in comparison with pure PCL/TCP scaffolds. It should be noted that although rapid prototyped scaffolds are 100% interconnected and highly porous with a very regular structure, a previous study reported fewer cells

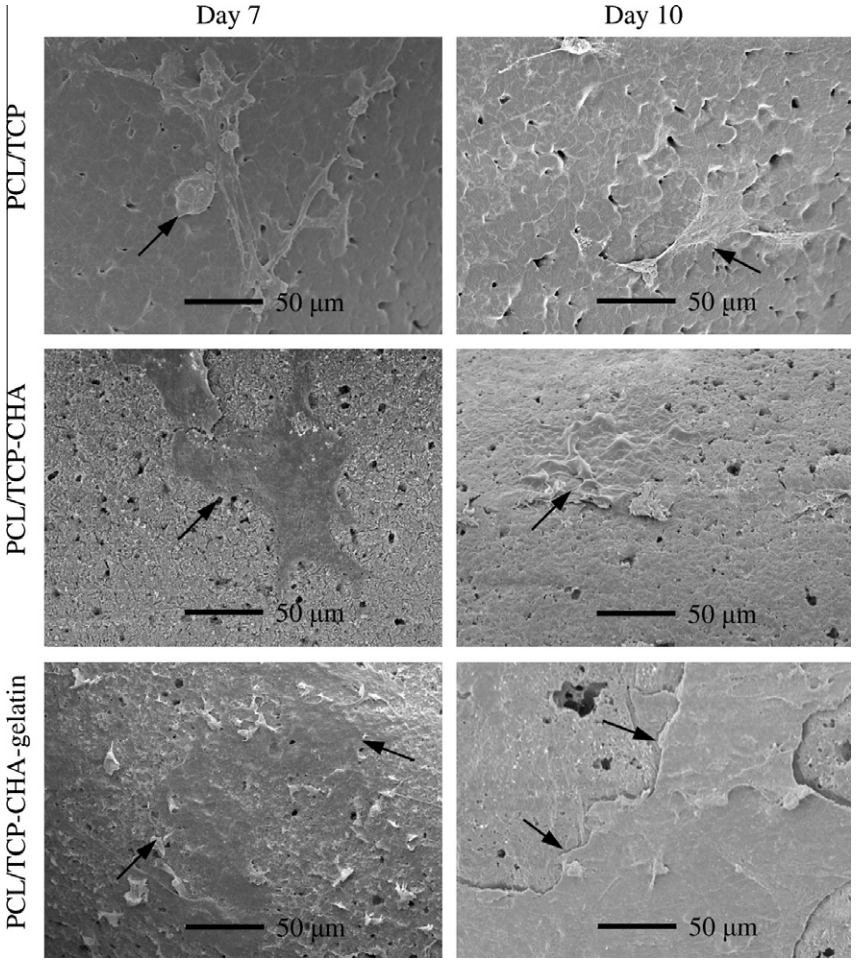

Fig. 6. SEM images of cell–scaffold constructs of PCL/TCP, PCL/TCP–CHA and PCL/TCP–CHA–gelatin scaffolds. The arrow indicates cells that have spread on surface of the scaffolds. The scale bar represents 50 μm.

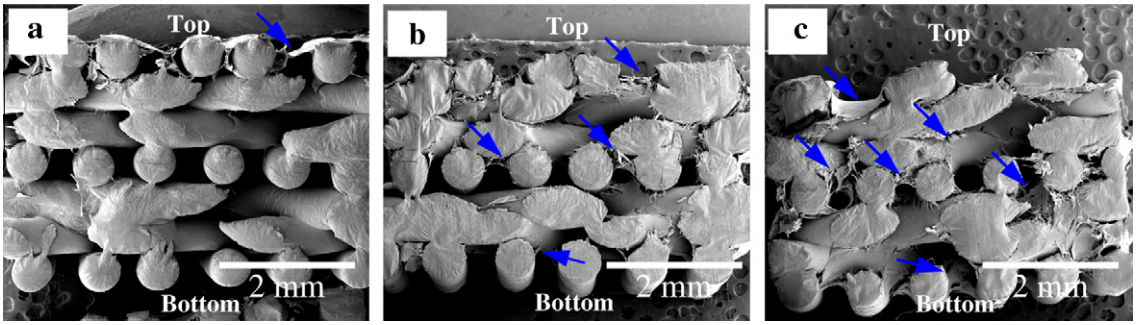

Fig. 7. SEM images of cross-sections of cell–scaffold construct at day 31. (a) PCL/TCP; (b) PCL/TCP–CHA, and (c) PCL/TCP–CHA–gelatin. Cells and the tissue sheet are indicated by arrows. The scale bar represents 2 mm.

and less tissue penetration into the interior of PCL/TCP scaffolds [9]. The incorporation of induction factors into the interior of the scaffolds has been proposed in order to obtain a uniform cell distribution throughout the scaffolds [9]. To study the influence of CHA–gelatin composite coating on the cell and tissue distributions within the interior of the scaffolds cross-sections of the cell–scaffold constructs on day 31 were analyzed using SEM (Fig. 7). Fewer cells and less tissue sheet formation were observed within PCL/TCP scaffolds, specifically within the interior of the scaffolds. In contrast, there was greater cell and tissue penetration into the interior of the coated scaffolds, especially the CHA–gelatin composite-coated scaffolds. The most even distribution of cells and tissues was found in the CHA–gelatin composite-coated scaffolds. Thus, the CHA–gelatin composite coating had a significant influence on cell and tissue distribution within the interior of the scaffolds.

The morphology, viability and cell distribution of BMSCs cultured on the scaffolds were also studied by confocal laser microscopy. As revealed in Fig. 8, on day 3 BMSCs were evenly distributed in the PCL/TCP–CHA–gelatin scaffolds and stretched over the pores. In contrast, qualitatively fewer BMSCs were observed in the PCL/TCP scaffolds and they had a more rounded morphology. Similar differences in cells distribution and morphology were observed on day 10. At all the time points more BMSCs were observed in the CHA–gelatin composite-coated scaffolds than in the CHA-coated scaffolds, indicating that gelatin in the composite coating played an important role in promoting cell distribution. These results are in agreement with the SEM results.

It should be noted that cells attached to and growing on the bars of rapid prototyped scaffolds experience different mechanical constraints in comparison with other types of scaffolds. In general, free tissue bridges formed within the adjacent bars exert a greater tensile force than would be expected for cells grown on foams or fibres, which attach individually to the supporting material. This tensile force due to the free tissue bridges could lead to flaking of the apatite layer from the bars of the scaffolds, as reported previously [16]. In contrast, the CHA–gelatin composite coating did not show any tendency to flake during cell culture, which demonstrates excellent adhesion of the biomimetic coating to the scaffolds. This could be due to the gelatin incorporated in the CHA–gelatin composite coating. A significantly higher retention of an apatite–collagen composite coating in comparison with an apatite coating was reported previously [17]. No flaking of the CHA–gelatin composite coating may also be due to the sub-micrometer coating thickness, in contrast to the few micrometers thick apatite coating investigated previously [16], as it is known that the critical load for coating delamination decreases with increasing coating thickness [17].

PicoGreen® is a fluorescent probe that binds proportionally to DNA [39]. The PicoGreen® results showed that on days 7 and 10 the PCL/TCP–CHA–gelatin scaffolds exhibited statistically significantly higher DNA contents ($P < 0.05$) compared with both the PCL/TCP and PCL/TCP–CHA scaffolds, as shown in Fig. 9. On day 10 the PCL/TCP–CHA–gelatin scaffold showed around 2.3 and 1.7 times higher amounts of DNA compared with the PCL/TCP and PCL/TCP–CHA scaffolds, respectively. At the same time, the PCL/TCP–CHA scaffold showed around a 1.3 times higher amount of DNA compared with the PCL/TCP scaffold. The R^2 value for the DNA content assay of the PCL/TCP–CHA–gelatin scaffolds was 0.997, which indicates that more cells were found to attach to and spread on the PCL/TCP–CHA–gelatin scaffold with increasing culture time. On the other hand, the R^2 values for the PCL/TCP–CHA and PCL/TCP scaffolds were 0.9739 and 0.833, respectively. The higher cell proliferation on the PCL/TCP–CHA–gelatin scaffold was because of the presence of gelatin in the coating, as gelatin has been recognized to promote cell proliferation [20]. Besides the chemical composition, the rough surface topography and high surface hydrophilicity of the PCL/TCP–CHA–gelatin scaffold could also improve the proliferation of BMSCs. Improvements in cell proliferation with increasing surface roughness and hydrophilicity has been reported previously [37,40].

The expression levels of osteogenic genes on days 17 and 24 were measured by RT-PCR. Fig. 10 shows that on day 17 the PCL/TCP–CHA and PCL/TCP–CHA–gelatin scaffolds had 1.7 and 1.1 times higher mean expression of core binding factor α1(Cbfa1), respectively, than the PCL/TCP scaffold. On day 24 Cbfa1 expression on the PCL/TCP–CHA and PCL/TCP–CHA–gelatin scaffolds was slightly lower compared with the PCL/TCP scaffold. Cbfa1 is an essential transcription factor for the commitment of multipotent mesenchymal cells to the osteoblastic lineage by triggering gene expression of bone matrix proteins [41,42]. It inhibits the transition of osteoblasts to osteocytes and thereby maintains osteoblastic cells at an immature stage and effectively directs the formation of immature bone. It is also know to inhibit adipocyte differentiation and promote endochondral ossification. Normally the expression of Cbfa1 is first detected in pre-osteoblasts and is up-regulated in immature osteoblasts, but down-regulated in mature osteoblasts [42,43]. Cbfa1 is also involved in regulating bone phenotypic genes, such as OCN [42,44,45]. As shown in Fig. 10, the expression of OCN, a terminal differentiation marker, was 1.12 and 1.6 times higher for the PCL/TCP–CHA and PCL/TCP–CHA–gelatin scaffolds, respectively, compared with OCN expression in cells on the PCL/TCP scaffold on day 24, when a slightly lower expression level of Cbfa1 was observed. Expression of collagen I (Col1), which relates to further BMSC differentiation to osteoblasts, showed slightly lower and basal expression levels for the PCL/TCP–CHA and PCL/TCP–CHA–gelatin scaffolds compared with uncoated PCL/TCP scaffolds on days 17 and 24. Down-regulation of Col1 expression in marrow stromal cells on hydroxyapatite after day 10 has also reported [46,47].

Western blotting was carried out to analyse protein extracts formed on cell–scaffold constructs after BMSCs were cultured for

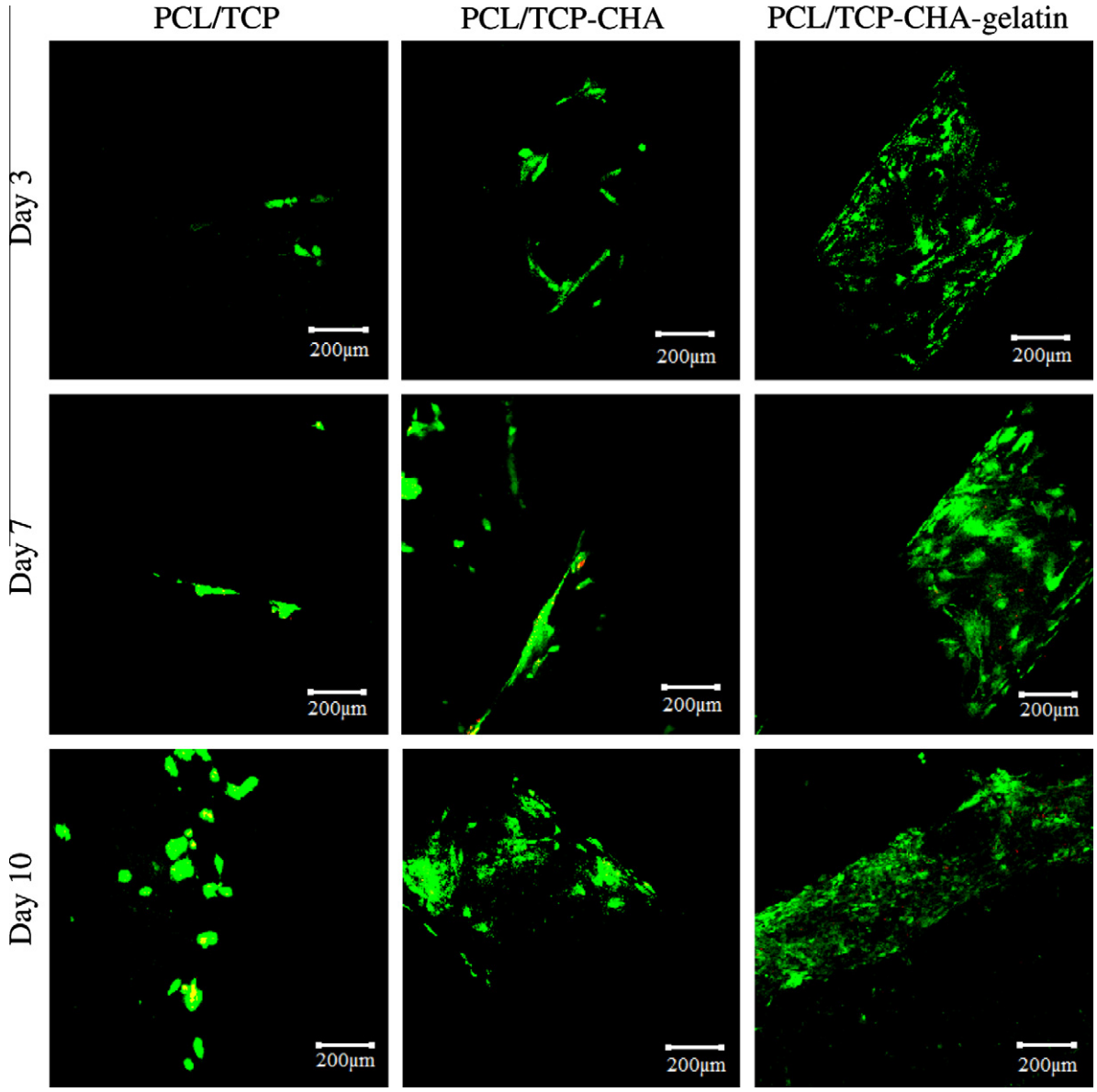

Fig. 8. Confocal laser microscopy with depth projection images reconstructed from multiple horizontal images shows the 3D distribution of cells within the scaffolds of PCL/TCP, PCL/TCP–CHA and PCL/TCP–CHA–gelatin. The scale bar represents 200 μm.

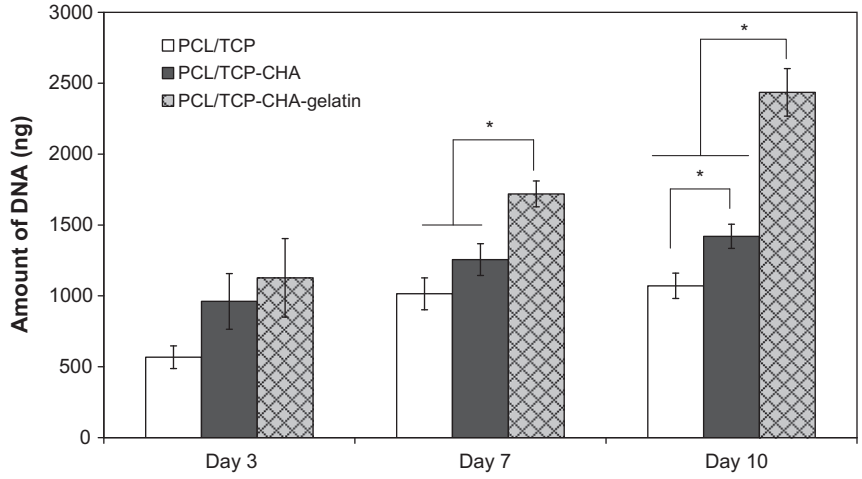

Fig. 9. PicoGreen® DNA quantification results for BMSCs cultured on PCL/TCP, PCL/TCP–CHA and PCL/TCP–CHA–gelatin scaffolds.

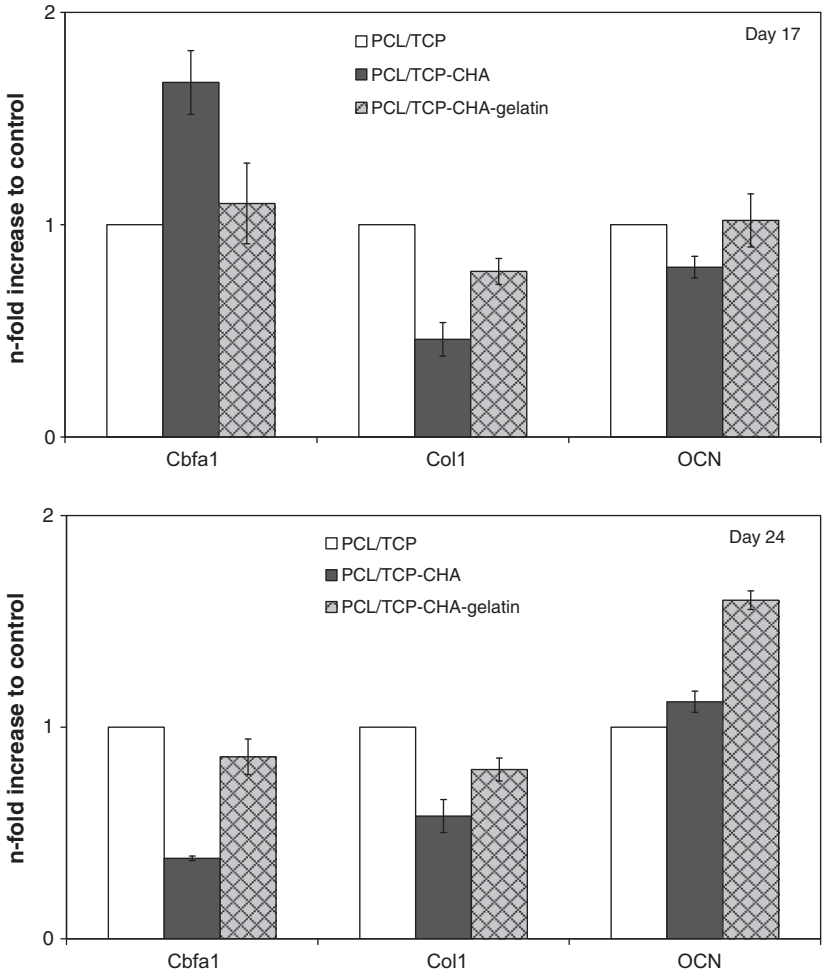

Fig. 10. Cbfa1, collagen I (Col1) and osteocalcin (OCN) mRNA expression in BMSCs cultured for 17 and 24 days on PCL/TCP, PCL/TCP–CHA and PCL/TCP–CHA–gelatin scaffolds.

31 days, and the results are shown in Fig. 11. ON is an important non-collagen calcium-binding glycoprotein secreted by osteoblasts and related to mineralization at the early stage of bone formation. The expression of ON was 1.7 and 1.4 times on the PCL/TCP–CHA–gelatin and PCL/TCP–CHA scaffolds, respectively, compared with that on PCL/TCP scaffolds. OCN is another non-collagenous protein which is most abundantly found in bone and dentin. This bone-specific glycoprotein is secreted by osteoblasts, binds to calcium and is known to promote calcification of the bone matrix. It has been used as a late marker for osteogenic differentiation and osteoblast maturation [38,42,48]. The expression of OCN was 1.6 and 1.5 times higher on the PCL/TCP–CHA–gelatin and PCL/TCP–CHA

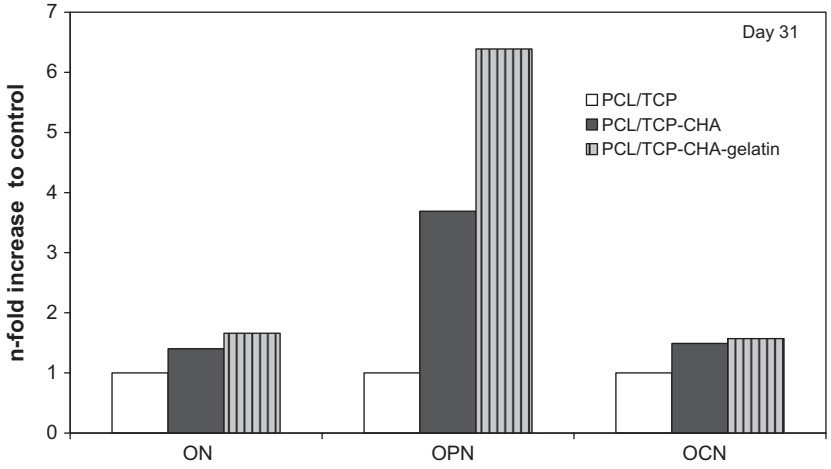

Fig. 11. Osteonectin (ON), osteopontin (OPN) and osteocalcin (OCN) protein extracts from cell–scaffold constructs after culture with BMSCs for 31 days on PCL/TCP, PCL/TCP–CHA and PCL/TCP–CHA–gelatin scaffolds.

scaffolds, respectively, compared with that on the PCL/TCP scaffold. OPN is another mineral-binding protein found in bone extracellular matrix (ECM) and could regulate crystal growth. It is associated with cell attachment, proliferation and biomineralization of ECM into bone and its expression demonstrates commitment of BMSCs to osteogenic differentiation [48]. A significantly higher level (6.4 times) of OPN expression was observed on the PCL/TCP–CHA–gelatin scaffold compared with that on the PCL/TCP scaffold. At the same time, the PCL/TCP–CHA scaffold showed 3.7 times higher OPN expression compared with the PCL/TCP scaffold.

Above all, in vitro western blotting testing showed higher ON, OPN and OCN expression on the PCL/TCP–CHA–gelatin scaffold compared with that on the PCL/TCP–CHA scaffold. The presence of gelatin in the CHA–gelatin composite coating may be the key factor in the stimulation of the osteogenic differentiation of BMSCs [49]. A previous study also showed that the addition of collagen to hydroxyapatite implants can enhance both phagocytotic and osteogenic processes [50]. These results suggest that PCL/TCP–CHA–gelatin scaffolds are more suitable for proliferation and osteogenic differentiation of BMSCs compared with PCL/TCP scaffolds, as well as PCL/TCP–CHA scaffolds.

4. Conclusions

In this study biomimetic CHA/gelatin composite-coated rapid prototyped scaffolds were developed, and the proliferation and osteogenic differentiation of BMSCs on these scaffolds were evaluated. Rapid prototyped PCL/TCP scaffolds were fabricated using an in-house SES. The fabricated PCL/TCP scaffolds exhibited a honeycomb structure with 100% interconnectivity and 65% porosity. In order to improve their osteoconductive properties the scaffolds were coated with a CHA–gelatin composite by a biomimetic co-precipitation process. PCL/TCP scaffolds coated with CHA alone were also prepared in order to understand the influence of gelatin on cell activity. The chemical structure of the coating was verified by XPS and ATR-FT-IR. Water contact angle measurement revealed improved hydrophilicity after coating. Moreover, the coating process did not have a detrimental effect on the mechanical properties of the scaffolds, as demonstrated by compression testing in dry and simulated physiological states. The thicknesses of the developed CHA and CHA–gelatin composite coatings were 600 and 800 nm, respectively. The CHA–gelatin composite coating did not show any flaking on the bars of the rapid prototyped PCL/TCP scaffolds during BMSC culture. SEM images of cross-sections showed that the most uniform distribution of cells within the interior of the cell–scaffold constructs was observed in the PCL/TCP–CHA–gelatin scaffold. PicoGreen® staining results showed that the proliferation rates of BMSCs on the PCL/TCP–CHA–gelatin scaffold were about 2.3 and 1.7 times higher than on the PCL/TCP and PCL/TCP–CHA scaffolds, respectively, on day 10. RT-PCR analysis showed that the PCL/TCP–CHA–gelatin scaffold had highest level of OCN on day 24. Cbfa1 levels were relatively higher for both the PCL/TCP–CHA scaffolds and PCL/TCP–CHA–gelatin scaffolds compared with the PCL/TCP scaffold at the early osteoblast stage and relatively lower at more mature stages. The expression of Col1 was unaffected, regardless of the type of coating. A Western blot study demonstrated that the PCL/TCP–CHA–gelatin scaffold had the highest levels of ON, OPN and OCN expression. These findings suggest that the CHA–gelatin composite coating was more effective than the CHA coating in improving the proliferation and osteogenic differentiation of porcine BMSCs on rapid prototyped scaffolds, which could be attributed to gelatin in the composite coating. This study suggests the potential application of biomimetic composite coatings on RP scaffolds. Consequently, the CHA–gelatin composite-coated PCL/TCP scaffold should be regarded as a promising rapid prototyped scaffold for bone tissue engineering.

Acknowledgment

Financial support for this research from the A*STAR Program under Grant No. R 397 000 038 305 is acknowledged.

Appendix A. Figures with essential colour discrimination

Certain figures in this article, particularly Figs. 2, 3, 4, 7 and 8, are difficult to interpret in black and white. The full colour images can be found in the on-line version, at doi:10.1016/j.actbio.2010.09.010).

References

[1] Ma PX. Scaffolds for tissue fabrication. Mater Today 2004;7:30–40.
[2] Hutmacher DW. Scaffolds in tissue engineering bone and cartilage. Biomaterials 2000;21:2529–43.
[3] Hutmacher DW, Cool S. Concepts of scaffold-based tissue engineering – the rationale to use solid free-form fabrication techniques. J Cell Mol Med 2007;11:654–69.
[4] Leong KF, Cheah CM, Chua CK. Solid freeform fabrication of three-dimensional scaffolds for engineering replacement tissues and organs. Biomaterials 2003;24:2363–78.
[5] Hutmacher DW, Sittinger M, Risbud MV. Scaffold-based tissue engineering: rationale for computer-aided design and solid free-form fabrication systems. Trends Biotechnol 2004;22:354–62.
[6] Hollister SJ. Porous scaffold design for tissue engineering. Nat Mater 2005;4:518–24.
[7] Wang F, Shor L, Darling A, Khalil S, Sun W, Guceri S, et al. Precision extruding deposition and characterization of cellular poly-ε-caprolactone tissue scaffolds. Rapid Prototyping J 2004;10:42–9.
[8] Shor L, Guceri S, Wen X, Gandhi M, Sun W. Fabrication of three-dimensional polycaprolactone/hydroxyapatite tissue scaffolds and osteoblast–scaffold interactions *in vitro*. Biomaterials 2007;28:5291–7.
[9] Zhou YF, Hutmacher DW, Varawan SL, Lim TM. *In vitro* bone engineering based on polycaprolactone and polycaprolactone–tricalcium phosphate composites. Polym Int 2007;56:333–42.
[10] Kretlow JD, Mikos AG. Mineralization of synthetic polymer scaffolds for bone tissue engineering. Tissue Eng 2007;13:927–38.
[11] Mann S, Archibald DD, Didymus JM, Douglus T, Heywood BR, Meldrum FC, et al. Crystallization at inorganic–organic interfaces: biominerals and biomimetic synthesis. Science 1993;261:1286–92.
[12] Kokubo T et al. Ca, P-rich layer formed on high strength bioactive glass–ceramic A–W. J Biomed Mater Res 1990;24:331–43.
[13] Xiong JY, Li YC, Wang XJ, Hodgson PD, Wen CE. Mechanical properties and bioactive surface modification via alkali-heat treatment of a porous Ti–18Nb–4Sn alloy for biomedical applications. Acta Biomater 2008;4:1963–8.
[14] Park IS, Choi UJ, Yi HK, Park BK, Lee MH, Bae TS. Biomimetic apatite formation and biocompatibility on chemically treated Ti–6Al–7Nb alloy. Surf Interface Anal 2008;40:37–42.
[15] LeGeros RZ. Biological and synthetic apatites. In: Brown PW, Constantz B, editors. Hydroxyapatite and related materials. Boca Raton, FL: CRC Press; 1994. p. 1–28.
[16] Chim H, Hutmacher DW, Chou AM, Oliveira AL, Reis RL, Lim TC, et al. A comparative analysis of scaffold material modifications for load-bearing applications in bone tissue engineering. Int J Oral Max Surg 2006;35:928–34.
[17] de Jonge LT et al. The osteogenic effect of electrosprayed nanoscale collage/calcium phosphate coatings on titanium. Biomaterials 2010;31:1–9.
[18] Chen Y, Mak AFT, Wang M, Li J. Composite coating of bonelike apatite particles and collagen fibers on poly L-lactic acid formed through an accelerated biomimetic coprecipitation process. J Biomed Mater Res Part B Appl Biomater 2006;77:315–22.
[19] Chang MC, Ko CC, Douglas WH. Preparation of hydroxyapatite–gelatin nanocomposite. Biomaterials 2003;24:2853–62.
[20] Kim HW, Kim HE, Salih V. Stimulation of osteoblast responses to biomimetic nanocomposites of gelatin–hydroxyapatite for tissue engineering scaffolds. Biomaterials 2005;26:5221–30.
[21] Liu X, Smith LA, Hu J, Ma PX. Biomimetic nanofibrous gelatin/apatite composite scaffolds for bone tissue engineering. Biomaterials 2009;30:2252–8.
[22] Landi E, Celotti G, Tampieri A. Carbonated hydroxyapatite as bone substitute. J Eur Ceram Soc 2003;23:2931–7.
[23] Arafat MT, Savalani MM, Gibson I. Improving the mechanical properties in tissue engineered scaffolds. In: Proceedings of the ASME international mechanical engineering congress and exposition. Boston, USA: Amer Soc Mechanical Engineers; 2008. p. 3–6.
[24] Oyane A, Uchida M, Choong C, Triffitt J, Jones J, Ito A. Simple surface modification of poly(epsilon-caprolactone) for apatite deposition from simulated body fluid. Biomaterials 2005;26:2407–13.
[25] Schumann D, Ekaputra AK, Lam CX, Hutmacher DW. Design of bioactive, multiphasic PCL/collagen type I and type II-PCL–TCP/collagen composite

scaffolds for functional tissue engineering of osteochondral repair tissue by using electrospinning and FDM techniques. Methods Mol Med 2007;140:101–24.
[26] Yeo A, Rai B, Sju E, Cheong JJ, Teoh SH. The degradation profile of novel, bioresorbable PCL–TCP scaffolds: an in vitro and in vivo study. J Biomed Mater Res A 2008;84:208–18.
[27] Blaker JJ, Gough JE, Maquet I, Notingher I, Boccaccini AR. In vitro evaluation of novel bioactive composites based on bioglass-filled polylactide foams for bone tissue engineering scaffolds. J Biomed Mater Res 2003;67:1401–11.
[28] Ishaug SL, Crane GM, Miller MJ, Yasko AW, Yaszemski MJ, Mikos AG. Bone formation by three-dimensional stromal osteoblast culture in biodegradable polymer scaffolds. J Biomed Mater Res 1997;36:17–28.
[29] Liao S, Ngiam M, Watari F, Ramakrishna S, Chan CK. Systematic fabrication of nano-carbonated hydroxyapatite/collagen composites for biomimetic bone grafts. Bioinsp Biomim 2004;2:37–41.
[30] Jongpoiboonkit L, Franklin-Ford T, Murphy WL. Mineral coated polymer microspheres for controlled protein binding and release. Adv Mater 2009;21:1–4.
[31] Mobini S, Javadpour J, Hosseinalipour M, Ghazi-Khansari M, Khavandi A, Rezaie HR. Synthesis and characterisation of gelatin–nano hydroxyapatite composite scaffolds for bone tissue engineering. Adv Appl Ceram 2008;107:4–8.
[32] Touny AH, Laurencin C, Nair L, Allcock H, Brown PW. Formation of composites comprised of calcium deficient HAp and cross-linked gelatin. J Mater Sci Mater Med 2008;19:3193–201.
[33] Combes C, Rey C. Adsorption of proteins and calcium phosphate materials bioactivity. Biomaterials 2002;23:2817–23.
[34] Boskey A, Camacho NP. FT-IR imaging of native and tissue engineered bone and cartilage. Biomaterials 2007;28:2464–78.
[35] Gupta D, Venugopal J, Mitra S, Giri Dev VR, Ramakrishna S. Nanostructured biocomposite substrates by electrospinning and electrospraying for the mineralization of osteoblasts. Biomaterials 2009;30:2085–94.
[36] Gu YW, Tay BY, Lim CS, Yong MS. Biomimetic deposition of apatite coating on surface-modified NiTi alloy. Biomaterials 2005;26:6916–23.
[37] Anselme K. Osteoblast adhesion on biomaterials. Biomaterials 2000;21: 667–81.
[38] Pittenger MF et al. Multilineage potential of adult human mesenchymal stem cells. Science 1999;284:143–7.
[39] Ng KW, Leong DT, Hutmacher DW. The challenge to measure cell proliferation in two and three dimensions. Tissue Eng 2005;11:182–91.
[40] Chen Y, Cho MR, Mak AFT, Li JS. Morphology and adhesion of mesenchymal stem cells on PLLA, apatite and apatite/collagen surfaces. J Mater Sci Mater Med 2008;19:2563–7.
[41] Komori T. Regulation of skeletal development by the Runx family of transcription factors. J Cell Biochem 2005;95:445–53.
[42] Komori T. Regulation of osteoblast differentiation by runx2. Adv Exp Med Biol 2010;658:43–9.
[43] Stein GS et al. Runx2 control of organization, assembly and activity of the regulatory machinery for skeletal gene expression. Oncogene 2004;23: 4315–29.
[44] Merriman HL et al. The tissue-specific nuclear matrix protein, NMP-2, is a member of the AML/CBF/PEBP2/runt domain transcription factor family: interactions with the osteocalcin gene promoter. Biochemistry 1995;34:13125–32.
[45] Banerjee C, McCabe LR, Choi JY, Hiebert SW, Stein JL, Stein GS, et al. Runt homology domain proteins in osteoblast differentiation: AML3/CBFA1 is a major component of a bone-specific complex. J Cell Biochem 1997;66:1–8.
[46] Sun H et al. The upregulation of osteoblast marker genes in mesenchymal stem cells prove the osteoinductivity of hydroxyapatite/tricalcium phosphate biomaterial. Transplant Proc 2008;40:2645–8.
[47] Muller P et al. Calcium phosphate surfaces promote osteogenic differentiation of mesenchymal stem cells. J Cell Mol Med 2008;12:281–91.
[48] Donzelli E et al. Mesenchymal stem cells cultured on a collagen scaffold: in vitro osteogenic differentiation. Arch Oral Biol 2007;52:64–73.
[49] Rim NG, Lee JH, Jeong SI, Lee BK, Kim CH, Shin H. Modulation of osteogenic differentiation of human mesenchymal stem cells by poly[(ι-lactide)–co-(ε-caprolactone)]/gelatin nanofibers. Macromol Biosci 2009;9:795–804.
[50] Rammelt S, Schulze E, Witt M, Petsch E, Biewener A, Pompe W, et al. Collagen type I increases bone remodelling around hydroxyapatite implants in the rat tibia. Cells Tissues Organs 2004;178:146–57.